Comparison of Numerical and Effective-Medium Modeling of Porosity in Layered Media

Istvan A. Veres, Robert A. Smith, and Valerie J. Pinfield

***Abstract*—In this study, modeling approaches for porosity in layered media are presented and compared. First, an effective-medium model is used to account for the frequency-dependent attenuation of the elastic waves. The effective-medium model is based on a single-scattering approach, i.e., it neglects multiple-scattering effects. Then, the effective-medium model is compared in time-domain finite element simulations. The numerical model allows the study of the scattering of the elastic waves on randomly distributed spherical cavities and also accounts for multiple-scattering effects. The models are compared to investigate the validity of the effective-medium model approach. The calculated reflected laminate responses and transmission spectra from the two models show a good agreement.**

I. Introduction

The evaluation of bulk-averaged porosity using ultrasonic techniques in composites, for example, has been pursued since the 1970s. The underlying physical principle is that the propagating ultrasonic waves are scattered at the randomly distributed pores, which leads to a frequency-dependent attenuation of the waves [1]. By measuring this attenuation and assuming identical, spherical scatters, the average volume fraction of the porosity can be evaluated. The measurement principle is independent of the investigated material and was successfully applied in composites [2] and also in aluminum castings [3]. This approach can be further improved by assuming scatterers with a particular distribution of radii and by inverting the parameters describing the distribution [4]. A slightly modified technique which assumes linearity in the attenuation with frequency was proposed for composites and tested on aluminum [5]. Investigations were not limited to metals, but were also extended to ceramics, for example [6], [7]. These approaches, however, have never been extended to layered structures such as glass laminate aluminum reinforced epoxy (GLARE). Within such fiber-metal laminates, the composite layers frequently suffer from porosity, which reduces the overall strength and performance of the laminate. Evidence of porosity is often seen in through-transmission ultrasonic C-scans, but there is no further information about the depth location and volume fraction of the porosity. To obtain this information, porosity must be modeled and described for each layer independently, which will be addressed in the presented paper.

The nature of the underlying physical effect of the attenuation, the scattering of ultrasound, strongly depends on the volume fraction of the cavities. In the most general case, the rescattering of waves and multiple-scattering effects are taken into account [8]. For low volume fractions, the latter is negligible [9] and the frequency-dependent attenuation can be directly calculated using the back-scattering of a single cavity, neglecting multiple-scattering events. In the resulting model, an effective complex wave number is used to account for the attenuation of the waves in a homogenized medium. Similarly, the elastic material properties such as density or wave velocities can be replaced by their effective counterparts. By using this approach, time- and frequency-domain responses of a homogenized model were compared with a discrete scatterer model [10], [11]. Although the homogenized model showed a good agreement with the discrete scatterer model, the latter neglected multiple scattering and, therefore, comparison for high filling fractions was not possible. The limits of the applicability of the homogenized model was studied in [12], showing that the different acoustic properties of a homogenized model might lead to reflections at the boundaries of the porous region.

Multiple scattering effects can also be treated by numerical simulations, as numerical techniques provide an excellent tool to study wave propagation problems in inhomogeneous, structured media. The finite element method (FEM), for example, allows the direct simulation and visualization of the scattering of the waves in a periodic medium [13]–[15]. The simulation of wave propagation through randomly-distributed scatterers, such as porosity, is more challenging, because a single configuration of scatterers might be insufficient to describe the average field [16] requiring a repetition of the simulation with different configurations or a spatial averaging of the simulated field. Numerical methods are nonetheless necessary tools to validate and compare the different approximations available to describe random media [16], [17] or to verify the existence of complex wave phenomena [18].

Manuscript received November 10, 2014; accepted January 18, 2015. Support is acknowledged from an ongoing Fellowship in Manufacturing of the UK Engineering and Physical Sciences Research Council (EPSRC; EP/K037315/1).

I. A. Veres and R. A. Smith are with the Department of Mechanical Engineering, University of Bristol, Bristol BS8 1TR, UK (e-mail: istvan.veres@recendt.at).

I. A. Veres is now with RECENDT GmbH, 4040 Linz, Austria.

V. J. Pinfield is with the Chemical Engineering Department, Loughborough University, Loughborough LE11 3TZ, UK.

DOI http://dx.doi.org/10.1109/TUFFC.2014.006837

In the presented work, the influence of the porosity is studied in layered structures by using analytical and numerical tools. The response of the layered structure is modeled by using the transfer-matrix method, whereby the effect of the porosity in the composite layer is taken into account by homogenized effective material properties [19]. Reflected laminate spectra and transmission spectra are calculated for various porosity levels and distributions. The results are compared with 3-D FEM simulations. The objective is to validate a rapid effective-medium model for use as an inversion tool to determine the depth distribution of porosity in layered structures.

II. Analytical and Numerical Modeling of Plane Wave Propagation in Layered Media

The response is described by a simple frequency-domain model. The porosity of the composite is taken into account by using a complex wave number for each layer, making it a homogenized effective medium. The 3-D time-domain FEM simulations are carried out by modeling the scattering of the ultrasonic waves at a random arrangement of spherical voids as a validation of the effective-medium model. The results of the two models are compared to verify and to investigate the limitations of the frequency-domain homogeneous model.

A. Frequency-Domain Response

For isotropic media, it is convenient to discuss acoustic problems by using elastic potentials [20], [21]. This formulism decouples the wave equation into dilatational (scalar) and rotational (vector) parts which fulfill the Helmholtz equations [(10) and (11) in the appendix]. The solution for wave propagation perpendicular to the surface of an arbitrary layer j in Cartesian coordinates can be given as a sum of forward- and backward-propagating longitudinal and shear waves, respectively:

$$\varphi^j = \chi[A_j e^{i(k_{lx}^j x)} + C_j e^{-i(k_{lx}^j x)}], \tag{1}$$

$$\psi_y^j = \chi[B_j e^{i(k_{tx}^j x)} + D_j e^{-i(k_{tx}^j x)}], \tag{2}$$

$$\text{with } \chi = e^{i(k_z z - \omega t)},$$

where the x-axis is the propagation direction and is perpendicular to the surface of the layers; the propagation constants are given as $k_{lx}^j = \sqrt{(k_l^j)^2 - k_z^2}$ and $k_{tx}^j = \sqrt{(k_{tx}^j)^2 - k_z^2}$ with k_l^j and k_t^j being the longitudinal and shear wave numbers in the jth layer, respectively; and k_z is the wave number parallel to the surface, which is equal in each layer. The general solution in (1) and (2) consists of 4 unknowns, A_j, B_j, C_j, and D_j, for each layer and 2 unknowns for the surrounding fluid on the incident or left-hand side (C^{L}) and transmitted or right-hand side (A^{R}) with $B^{\mathrm{R}} = D^{\mathrm{L}} = 0$, which can be evaluated by satisfying the continuity conditions between the layers. The system of linear equations can be reduced to the two unknown amplitudes (A^{R} and C^{L}, the reflected and transmitted fields) by using the transfer-matrix method [23]–[27] in Cartesian coordinates (intermediate steps are shown in the appendix). The rearranged equation is given in the following form:

$$\begin{bmatrix} A^{\mathrm{R}} \\ C^{\mathrm{L}} \end{bmatrix} = \begin{bmatrix} R_{11} & -K_{13}^N \\ R_{31} & -K_{33}^N \end{bmatrix}^{-1} \begin{bmatrix} K_{11}^N \\ K_{31}^N \end{bmatrix}, \tag{3}$$

where $\mathbf{R} = \mathbf{T}\mathbf{K}^1|_{x=x_0}$, $\mathbf{K}^N$ is evaluated at $x = x_{N-1}$: $\mathbf{K}^N = \mathbf{K}^N|_{x=x_{N-1}}$, and $\mathbf{T}$ is given in (18) in the appendix.

The reflected laminate responses of GLARE composite, submerged in water, with one and 10 composite layers, without porosity, are shown in Fig. 1. The aluminum and composite layers have thicknesses of 400 μm and 250 μm, respectively. For the calculations, an isotropic medium was used for the aluminum layers, and the composite layers are also approximated as isotropic media (the presented work deals only with normally incident longitudinal waves).[1] The responses in Fig. 1 can also be interpreted as reflection coefficients. In Fig. 1(b), for some frequency ranges (∼3 to 5 MHz or ∼10 to 12 MHz, for example) the reflection coefficient is 1, which indicates the presence of stop bands, a common effect in periodic media [13].

Next, the effect of the porosity will be taken into account in the model. It is convenient to describe the influence of the porosity by using effective-medium theories. This approach homogenizes the system by averaging over a particle distribution and assumes a complex wave number [10], [11] which accounts for the attenuation of the waves. This effective wave number K is given as

$$K^2 = k^2 + \frac{3\phi}{R^3} f(0), \tag{4}$$

where ϕ denotes the void volume fraction, k is the wave number, and $f(0)$ is the forward-scattered amplitude. For simplicity, it is assumed that the pores are spherical scatterers with radius R. The scattered amplitude in a direction θ can be obtained as [11]

$$f(\theta) = \frac{1}{ik} \sum_{n=0}^{\infty} (2n+1) A_n P_n(\cos(\theta)), \tag{5}$$

where A_n are the scattering coefficients from a spherical cavity and P_n is the Legendre polynomial of order n. The scattering of plane waves from spherical obstacles, such as cavities or inhomogeneities, is a well-known problem and it is discussed in detail in the literature for dilatational waves [20] and also for transverse waves [22]. For

[1] An isotropic aluminum is assumed with density ρ and bulk wave velocities (c_{l}, c_{s}) given as $\rho = 2700$ kg·m^{-3}, $c_{\mathrm{l}} = 6119$ m·s^{-1}, and $c_{\mathrm{s}} = 3103$ m·s^{-1}. Water is modeled as a nonviscous fluid with density ρ and bulk wave velocities (c_{l}, c_{s}) given as $\rho = 1000$ kg·m^{-3}, $c_{\mathrm{l}} = 1496$ m·s^{-1}, and $c_{\mathrm{s}} = 0$ m·s^{-1}. The material properties of the composite are given with the density ρ and bulk wave velocities (c_{l}, c_{s}) as $\rho = 1800$ kg·m^{-3}, $c_{\mathrm{l}} = 3330$ m·s^{-1}, and $c_{\mathrm{s}} = 1780$ m·s^{-1}.

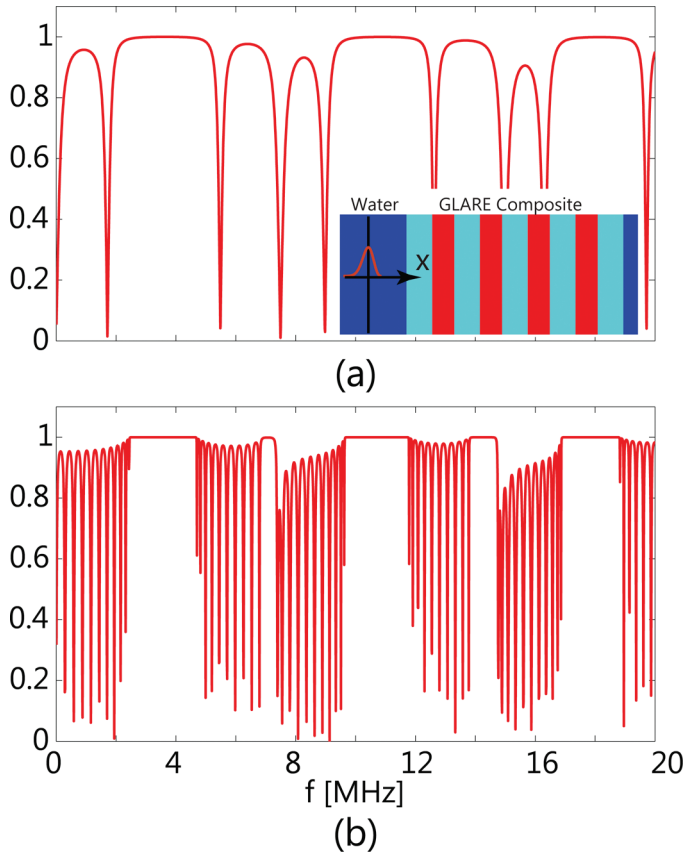

Fig. 1. Reflected laminate responses of a GLARE composite (a) with 1 and (b) with 10 composite layers without porosity. The responses can be interpreted as reflection coefficients which are 1 within stop bands. The inset in (a) shows a diagram of the investigated GLARE composite; the laminates are composed of alternating layers of aluminum and glass-fiber.

transverse waves, the definition of the scattering cross-section in (5) is slightly different because of the presence of two transverse waves with different polarization [22]. The infinite sum in (5) can be truncated; in the current work 15 Bessel components were used, which provides sufficient accuracy up to 100 MHz for the current system with a pore radius of $R \approx 10$ μm and wavelength of $\lambda \approx 19$ μm.

The presence of spherical voids in the elastic solid also reduces the stiffness and density of the material. The effective density of the medium is obtained as [11]

$$\rho_{\text{eff}} = \rho\left[1 + \frac{3\phi}{2k^2R^3}(f(0) - f(\pi))\right], \tag{6}$$

and the elastic material properties are also replaced by their frequency-dependent effective counterparts as

$$\mu_{\text{eff}} = \frac{\omega^2\rho_{\text{eff}}}{K_{\text{t}}^2}, \quad \lambda_{\text{eff}} = \frac{\omega^2\rho_{\text{eff}}}{K_{\text{l}}^2} - 2\mu_{\text{eff}}, \tag{7}$$

where K_{l} and K_{t} are the effective longitudinal and shear-wave numbers from (4), assuming either an incident longitudinal or shear wave, respectively.

In real-life samples, the distribution of the radii of the cavities is usually nonuniform and the overall attenuation must be evaluated [4]. For an average void volume fraction of $\bar{\phi}$, the overall attenuation is the sum of the imaginary parts of the effective wave numbers for each of the ith discrete pore sizes:

$$\alpha_{\text{eff}} = \sum_i K_i^{\text{imag}}, \tag{8}$$

where the complex wave numbers K_i are calculated for discrete radii r_i with the corresponding volume fractions ϕ_i:

$$\phi_i = \bar{\phi}\frac{r_i^3}{\sum_i r_i^3}. \tag{9}$$

These relatively simple relationships are used in the homogenized layers in the transfer-matrix method for the layered material, using (21) in the appendix to account for the porosity in the individual composite layers. The influence of the porosity on the frequency response of the layered medium will be investigated by using this model, and compared with 3-D time-domain FEM simulations.

B. Time-Domain Simulations of Wave Propagation in a Porous Layer

The time-domain FEM model is used for the direct simulation of the scattering of the ultrasonic waves and for a qualitative comparison with the analytical effective-medium model. For this purpose, the commercial FEM package PZFlex (Weidlinger Associates Inc., Mountain View, CA) was used and the applied model is shown in Fig. 2(a).

The pores in the composite layer are modeled as randomly-distributed spherical voids, as shown in Fig. 2(a). The spherical voids were arranged as follows: a 3-D cuboid lattice (87.5 × 87.5 × 50 μm) was created and each pore was randomly positioned around one of the centers of these cuboid cells; the maximal distance to the center is the length of the cell, which also allows the intersection of the voids. An incident plane wave was generated in water [the corresponding plane is at the height of point A in Fig. 2(b)], whereby the temporal dependence is given as: $f(t) = A(t^3/\upsilon^4)e^{(-2t^2)/\upsilon^2}$ with $\upsilon = 20$ ns and A is an arbitrary constant. This shape results in a reasonably flat frequency spectrum below 20 MHz which can be straightforwardly deconvolved after the simulation. The propagation path of the pulse is shown for one lateral position across the layers in Fig. 2(b). The figure visualizes the multiple reflections at the boundaries (at $x = 2.40$ mm and at $x = 2.65$ mm) of the layers and the scattering of the pulse in the porous composite layer.

At the boundaries in the y- and z-directions, symmetric boundary conditions (BCs) were used; along the x-direction, at both ends, absorbing BCs were applied. The water regions at the top and bottom of the model were, however, sufficiently large to exclude reflections from these bound-

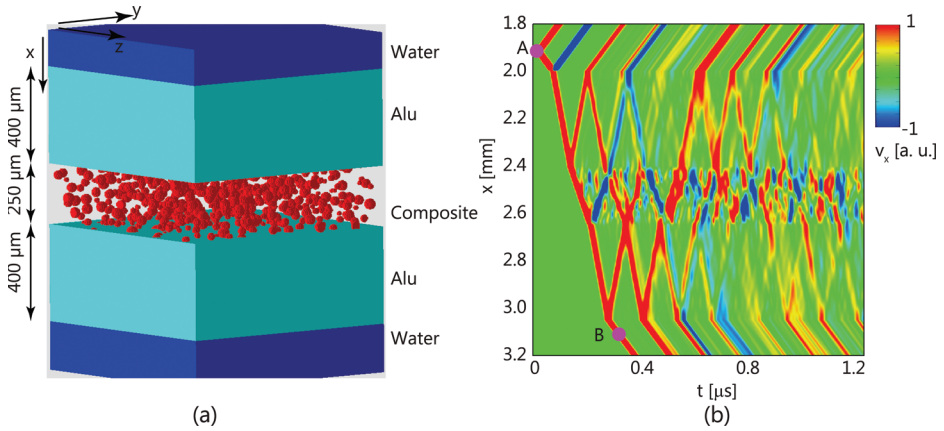

Fig. 2. (a) 3-D FEM model of the GLARE composite, consisting of two aluminum layers and a porous composite layer (for improved visibility of the pores, the image shows the pores as red inclusions in a transparent material; in the simulations, the shown spherical particles are voids in the composite material). (b) Multiple reflections of the positive-going half-cycle pulse propagating from the pink dot at A ($x = 1.9$ mm and $t = 0$), for one lateral position across the layers. Color represents particle velocity, where red is positive and blue is negative. The scattering of the waves at the pores in the middle composite layer is clearly visible between $x = 2.40$ mm and $x = 2.65$ mm. Note that the positive (red) pulse becomes negative (blue) when reflected at a boundary to an increasing impedance because this is a plot of particle velocity, not pressure.

aries within the first 4 µs of the simulation. The efficiency of the simulation was increased by successively growing the element dimensions in water toward both ends of the model (along the x-direction) by ~1% in each row.

The time-domain results of the 3-D FEM simulations were converted into frequency-domain responses by pursuing two different approaches. Either the frequency response—the reflected laminate spectrum—was evaluated, or the frequency-dependent attenuation of the waves, represented by the transmitted spectrum. Because the description of the random scattering problem requires the determination of mean values of the wave propagation, the captured responses were averaged across the cross-section of the models in the y–z plane.

The frequency response—reflected laminate spectrum—was determined by capturing the reflected and scattered waves in the time domain at the height of point A and by evaluating its frequency spectrum [Fig. 3(a)]. Simulations were carried out for both cases: with porous and with nonporous composite layers. In the nonporous case, the cross section of the investigated region was 0.1875 × 0.1875 mm. The element dimensions were $\Delta x = 2$ µm and $\Delta y = \Delta z = 2.6$ µm with a total of 95.8×10^6 elements [corresponding to a discretization with 287.4×10^6 degrees of freedom (DOF)]. In the calculations, pore radii of $R \approx 10$ to 16 µm are assumed and the wavelength at 50 MHz is $\lambda \approx 137$ µm, hence, $R \ll \lambda$. In the elastic, nonporous case, a simple 1-D model is sufficient to model normal incidence. Nonetheless, to check the overall quality of the model (such as numerical dispersion and the evaluation of the frequency response), we carried out a simulation with discretization and dimensions comparable with the porous case.

In the simulation with the porous layer, the modeled cross section of the GLARE composite was 0.975 × 0.975 mm. The element dimensions remained the same with $\Delta x = 2$ µm and $\Delta y = \Delta z = 2.6$ µm with a total of 181×10^6 elements (corresponding to a discretization with 542×10^6 DOF). Because of the larger cross-section, the total length of the model was shortened in the x-direction from 6.55 mm (nonporous case) to 4.55 mm to keep the dimensions and the necessary computational resources of the model within reasonable limits (i.e., DOF ~ 550×10^6). This length allows only 2.5 µs simulation time without reflection from the ends in the x-direction. Within the composite layer, 726 spherical scatterers with a radius of 16 µm were randomly distributed, whereby the total volume fraction of the pores was 4.7%.

III. Results and Discussion

A. Comparison of the Models

First the frequency response—reflected laminate spectrum—was determined. Simulations were carried out for both cases: with porous and with nonporous composite layers [Figs. 3(b) and 3(c)]. The time-domain responses captured at the height of point A (Fig. 2) are shown in the top row in Figs. 3(b) and 3(c). The normalized frequency spectra, or reflected laminate responses, in the bottom row of Figs. 3(b) and 3(c) are evaluated by the Fourier transform of these signals. In the nonporous case, the analytical and the numerical responses show an excellent agreement up to 25 to 30 MHz but deviations in the amplitude become visible for higher frequencies. In this case, the system did not include damping and the analytical solution is dominated by sharp, easily distinguishable resonances in the response. For the porous case, in the analytical solution, the real wave number was replaced by an effective, complex wave number (4). Hence, the waves are attenuated, which mimics the effect of the scattering of ultrasound. This is visible as the broadening of the resonances and as a frequency-dependent decrease

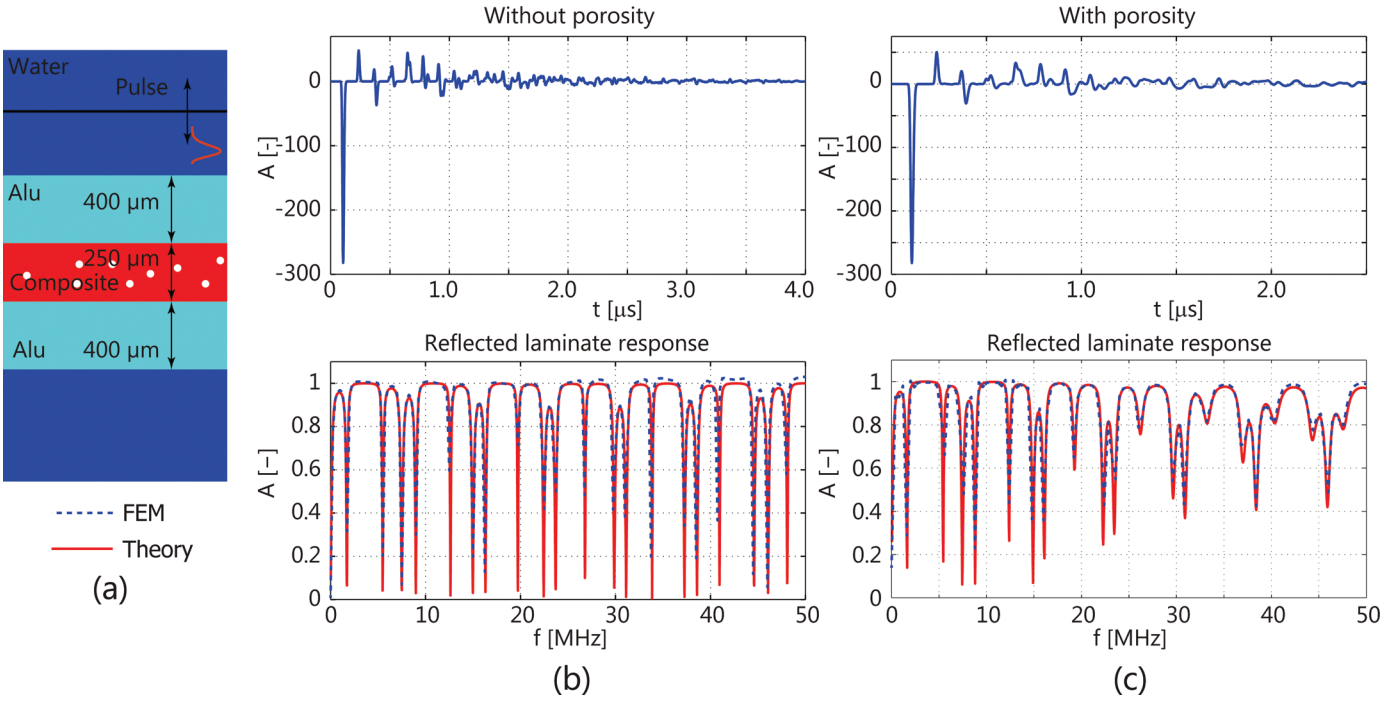

Fig. 3. (a) Model of the GLARE composite used in the comparison of the FEM simulations and the effective-medium model. (b) Captured time-domain waveform from the FEM simulation and its Fourier transform for the nonporous case compared with the effective-medium model. (c) Time-domain waveform (FEM model) and its Fourier transform for the porous layer compared with the effective-medium model.

of the amplitudes. The exact attenuation coefficient calculated from the effective-medium model is discussed and shown in the following subsection. The comparison of the effective-medium model with the FEM simulation proves, however, that the simple homogenized model is capable of describing the frequency-dependent attenuation of the waves caused by the scattering of the waves.

As an additional verification of the FEM model, simulations with different random void locations were performed.[2] The goal of the simulations was to verify that the averaged transmission spectra from the different configurations are comparable—i.e., the averaged responses are identical—and, therefore, that the presented method can be used to describe the response. From these simulations, the transmitted spectrum, or the frequency-dependent attenuation of the waves, was calculated. The simulated time-domain responses were averaged across the simulated cross section, and the resulting input and transmitted signals are shown in Fig. 4(a). The strong attenuation of the pulse is due to the impedance mismatch between aluminum and composite, which leads to a strong reflection of the waves. The normalized frequency spectra show the variation of the frequency spectra between the input and the transmitted pulses [Fig. 4(b)], which is the result of the scattering of the waves at the voids (porosity) in the composite layer. The division of the two spectra results in the transmission spectra. The comparison of the spectra from the different configurations indicates that the investigated system contains a sufficient number of scatterers to characterize it as a homogenized model.

B. Influence of the Pore Diameter and the Volume Fraction

Next, different pore diameters and volume fractions were studied.[3] The transmission spectra in Fig. 4(c) of the three systems with radii $R = 10$, 16, and 20 μm were evaluated from the FEM simulation similarly to the previous simulations using the spatially averaged time-domain responses. The comparison with the effective-medium model shows that this model is a good approximation of the numerical simulation for the cases with radii $R = 10$ and 16 μm (total volume fractions of 1.1%, 4.7%). For the largest diameter, $R = 20$ μm, with a total volume fraction of 9.4%, a deviation starts to become visible as the effective-medium model underestimates the attenuation.

In further simulations, the effect of varying the pore diameter was studied. In these simulations two ranges of pore diameters were used $R = 7.5$ to 22.5 μm and $R = 0$ to 30 μm both with a uniform distribution of the diameters and

[2] Three simulations were performed, each with 726 randomly arranged spherical scatterer with radii $R = 16$ μm. The arrangements were different in all cases. Similarly to the previous simulation, intersection of the spheres was allowed, leading to total volume fractions of 4.66%, 4.40%, and 4.54%. The models consisted of 181×10^6 elements, corresponding to 542×10^6 DOFs.

[3] Three simulations were performed, each with 726 randomly arranged spherical scatterer with radii $R = 10$, 16, or 20 μm. The geometric arrangements remained identical in all cases—i.e., the location of the pores remained the same, only the diameter was increased—leading to total volume fractions of 1.1%, 4.7%, and 9.4%, respectively. Similarly to the previous simulations, intersection of the spheres was allowed and the models consisted of 181×10^6 elements, corresponding to 542×10^6 DOFs.

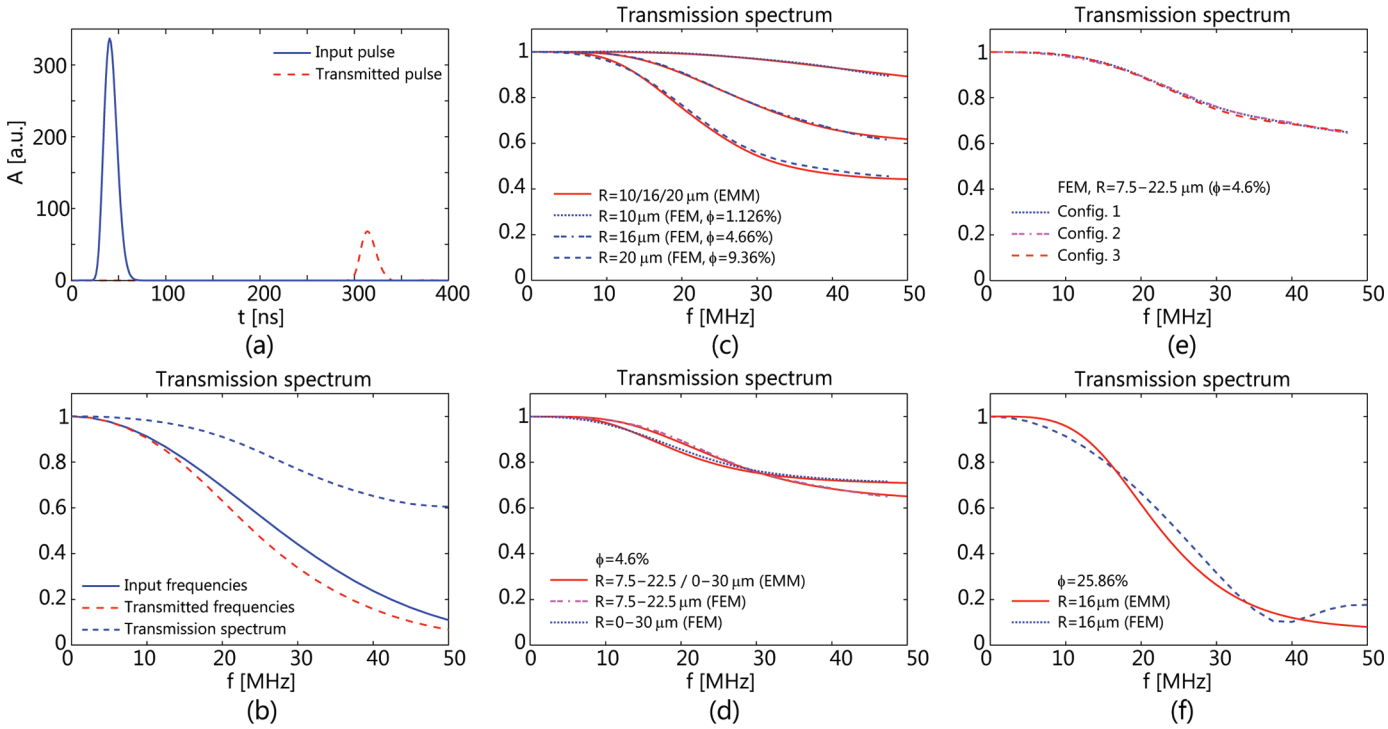

Fig. 4. (a) Input and transmitted time-domain pulses for the FEM model in the GLARE composite. (b) Frequency spectrum of the input and transmitted pulses in (a) and comparison of the transmission spectra from FEM simulations. (c) Analytical and numerical transmission spectra for three different scatterer diameters and volume fractions. (d) Transmission spectra from two FEM simulations with identical volume fractions but different scatterer diameter distributions, compared with the effective-medium model (EMM). (e) Comparison of the transmission spectra from three FEM simulations with identical pore volume fractions and different geometrical configurations. (f) Transmission spectra from a simulation with large volume fraction (25.9%) compared with the effective-medium model.

with the same total void volume fraction.[4] The attenuation coefficients for the effective-medium model were calculated with the help of (9), and a comparison with the FEM models is shown in Fig. 4(d). The effective-medium model is a good approximation of the FEM solution in this case as well. By comparing the two curves, it is clearly visible that the broader diameter distribution leads to a stronger attenuation for lower frequencies but the curve flattens out with a higher transmission coefficient. This property might allow a unique determination of the volume fraction or the diameter distribution from an inverse problem if one of these properties is known and measurement data are available for sufficiently high frequencies. For the first range of pore sizes, $R = 7.5$ to 22.5 μm, the simulations were also verified with three different configurations [Fig. 4(e)], justifying the validity of the simulations. Finally, a simulation with high void volume fraction ($\phi = 25.86\%$, $R = 16$ μm) was also carried out and compared with the prediction of the effective-medium model. The transmission spectrum in Fig. 4(f) shows the different predictions of the FEM model and the approximation using a complex wave number. This difference can be explained by the combination of the error due to neglecting multiple scattering events and the intersections of the pores in the FEM model, which leads to non-spherical scatterers.

By using the effective-medium model, the reflected laminate response was calculated for a single composite layer between two aluminum layers with varying the volume fractions (Fig. 5). In the calculations, single pore radii ($R = 10$, 16, and 20 μm) were used with three different volume fractions: 1%, 5%, and 10%. The comparison of the responses with the effective medium to the response without porosity (0% porosity is in green) show that for low volume fractions (~1%) the attenuation is rather negligible but the softening of the material leads to a clear shift in the resonance frequencies and the response also broadens. The attenuation increases with increasing volume fractions (5%, 10%) for frequencies above ~20 to 30 MHz. The position of particular resonance frequencies also shifts—such as the resonance frequency around 26 MHz. This property might be useful to evaluate the porosity in individual layers within a multilayer composite.

IV. Conclusion

In the presented paper, an analytical model and a numerical model were utilized to study the influence of the porosity in a multilayer composite. Effective material properties were applied within a transfer-matrix-based approach to take the porosity into account. The attenu-

[4] In the first case ($R = 7.5$ to 22.5 μm), 726 spheres [in the second case ($R = 0$ to 30 μm), 486 spheres] were randomly arranged, leading to total volume fractions of 4.62% and 4.59%, respectively. Similarly to the previous simulations, intersection of the spheres was allowed and the models consisted of 181×10^6 elements, corresponding to 542×10^6 DOFs.

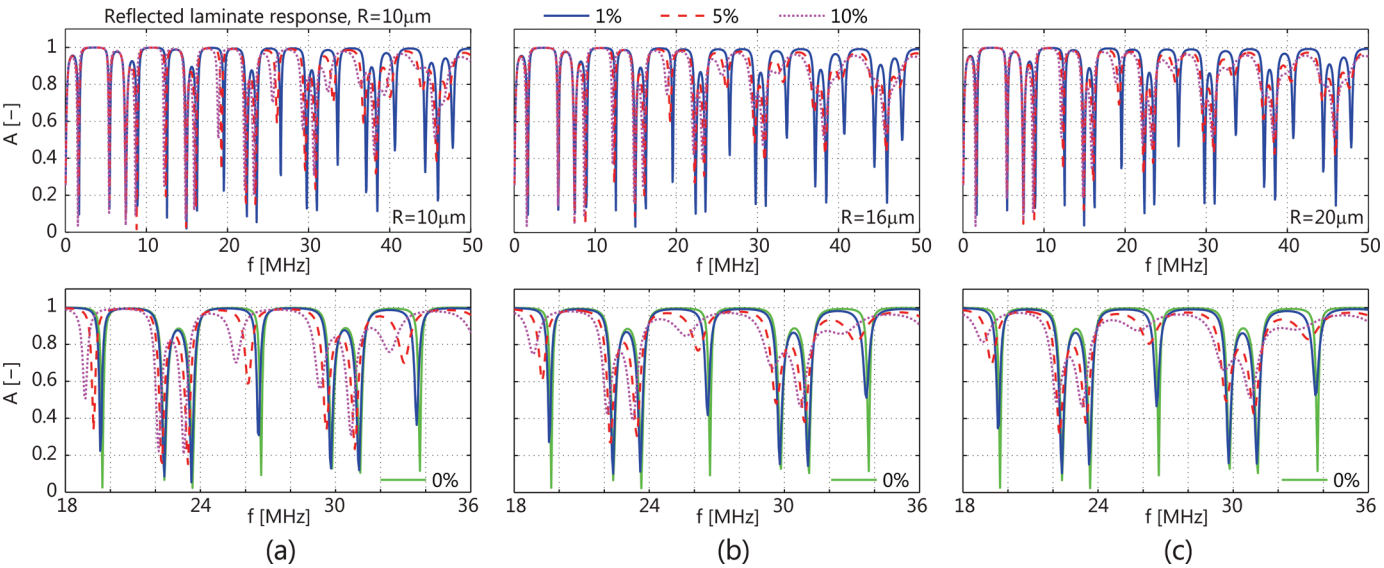

Fig. 5. Influence of the void volume fraction on the reflected laminate response with different pore radii predicted by the effective-medium model: (a) $R = 10$ μm, (b) $R = 16$ μm, and (c) $R = 20$ μm. Three different void volume fractions were investigated by using the analytic model, 1%, 5%, and 10%, plotted as blue solid, red dashed, and magenta dotted curves, respectively. The expanded portions of the frequency range from 18 to 36 MHz in the bottom row, including 0% in green, show that the increasing radius of the pores leads also to an increased attenuation with the same void volume fraction. This is visible through the broadening of the resonance peaks.

ation of the waves through scattering was also evaluated by 3-D FEM simulations. The resulting reflected laminate responses and transmission spectra of the two models were compared to investigate the limitation of the effective-medium model.

The effective-medium model neglects multiple scattering effects but these are taken into account in the 3DFEM simulations. The calculated reflected laminate responses and transmission spectra from the two models show a good agreement for porosity values below 20%. The comparison of the models included different pore diameters, volume fractions, and pore-diameter distributions. The comparison of the responses shows the attenuation and softening effects of the porosity on the response of the layered structure. The results show that the effective-medium model allows the approximation of the effect of the porosity for reasonable levels of volume fractions, below and around 10%.

Appendix
Transfer-Matrix Method for a Layered Structure Submerged in Fluid

For isotropic media, it is convenient to discuss acoustic problems by using elastic potentials [20], [21]. This formulism decouples the wave equation into dilatational (scalar) and rotational (vector) parts which fulfill the Helmholtz equations:

$$(\Delta + k_{\mathrm{l}}^2)\varphi = 0, \tag{10}$$

$$(\Delta + k_{\mathrm{t}}^2)\mathbf{\Psi} = 0, \tag{11}$$

where Δ denotes the Laplacian and φ and $\mathbf{\Psi}$ are the scalar and the vector potentials, respectively. The wave numbers k_{l} and k_{t} correspond to the longitudinal and shear waves represented by these potentials. Because plane waves can be reduced to two spatial dimensions, the problem involves only the scalar components and one vector component, φ and ψ_y in the investigated case.

In layered media, these equations must be fulfilled in each layer. The solution in Cartesian coordinates for an arbitrary layer j can be given as a sum of incident and reflected longitudinal and shear waves [see (1) and (2)] and the corresponding displacements are given as

$$\mathbf{u} = \nabla\varphi + \nabla \times \Psi. \tag{12}$$

The incident wave in the surrounding matrix can also be described as a harmonic wave. In the following, a nonviscous fluid matrix will be considered with an incident longitudinal wave with amplitude A_0 described as

$$\varphi^{\mathrm{inc}} = \chi A_0 e^{i(k_{\mathrm{l}x}^j x)}. \tag{13}$$

The unknowns A_j through D_j in (1) and (2) can be evaluated by satisfying the boundary conditions between the subsequent layers, given as the continuity of the stresses and displacements between the jth and $(j-1)$th layers:

$$u_x^{j-1} = u_x^j, \quad u_z^{j-1} = u_z^j, \tag{14}$$

$$\sigma_{xx}^{j-1} = \sigma_{xx}^j, \quad \sigma_{xz}^{j-1} = \sigma_{xz}^j. \tag{15}$$

The stresses σ_{ij} and strains ε_{kl} are given by the constitutive equation as

$$\sigma_{ij} = c_{ijkl}\varepsilon_{kl} = \frac{1}{2}c_{ijkl}\left(\frac{\partial u_k}{\partial x_l} + \frac{\partial u_l}{\partial x_k}\right). \tag{16}$$

For a multilayered system, (14) and (15) lead to an impractically large system of equations. Because the displacements and stresses in the intermediate layers are not required, the application of the so-called transfer matrix method is appropriate. Besides the classical transfer matrix formalism for isotropic [23] and anisotropic layers [24], the stiffness matrix method [25]–[27] has also been developed. In the current work, a Cartesian formulism of a simple transfer matrix approach will be used based on [23]. Correspondingly, the relevant unknown displacements and stresses in the jth layer ($x^{j-1} \le x \le x^j$) can be collected in a matrix form as

$$[u_x, u_z, \sigma_{xx}, \sigma_{xz}]^{\mathrm{T}} = \mathbf{K}^j[A_j, B_j, C_j, D_j]^{\mathrm{T}}. \tag{17}$$

The components of $\mathbf{K}^j$ can be found by substituting (1) and (2) into (12)–(16).

The transfer matrix of the jth layer relates the displacements and stresses at the left (x_{j-1}) and right boundaries (x_j) of the jth layer and it is defined as $\mathbf{T}^j = \mathbf{K}^j\big|_{x=x_j}(\mathbf{K}^j\big|_{x=x_{j-1}})^{-1}$. The total transfer matrix of the layered media can be found as the product of the transfer matrices of the individual layers:

$$\mathbf{T} = \prod_{j=1}^{N-2}\mathbf{T}^{N-j}, \tag{18}$$

which relates the unknown fields at the boundary $x = 0$ to the fields at the boundary $x = x_{N-1}$ as

$$[1,0,C^{\mathrm{L}},D^{\mathrm{L}}]^{\mathrm{T}} = \mathbf{S}_n[A^{\mathrm{R}},B^{\mathrm{R}},0,0]^{\mathrm{T}}, \tag{19}$$

with $\mathbf{S} = (\mathbf{K}^N\big|_{x=x_{N-1}})^{-1}\mathbf{T}_x\mathbf{K}^1\big|_{x=x_0}$. Because the layered plate is submerged in a nonviscous fluid (water), further straightforward modifications of the original technique can be carried out. For a nonviscous fluid matrix, the shear stresses must vanish at the outer boundary and in the fluid matrix only the scalar potential with one unknown constant exists ($B^{\mathrm{R}} = D^{\mathrm{L}} = 0$). Because the continuity of u_z at the outer boundary cannot be satisfied, only two equations can be applied in (19) to describe the continuity of the fields:

$$\begin{bmatrix} K_{11}^N & K_{13}^N \\ K_{31}^N & K_{33}^N \end{bmatrix}\begin{bmatrix} A^0 \\ C^{\mathrm{L}} \end{bmatrix} = \begin{bmatrix} R_{11} \\ R_{31} \end{bmatrix}[A^{\mathrm{R}}], \tag{20}$$

where $\mathbf{R} = \mathbf{T}\mathbf{K}^1\big|_{x=x_0}$ and $\mathbf{K}^N$ is evaluated at $x = x_{N-1}$: $\mathbf{K}^N = \mathbf{K}^N\big|_{x=x_{N-1}}$. The two remaining unknown amplitudes (A^{R} and C^{L} with $A^0 = 1$) can be found by solving the rearranged equation:

$$\begin{bmatrix} K_{11}^N \\ K_{31}^N \end{bmatrix} = \begin{bmatrix} R_{11} & -K_{13}^N \\ R_{31} & -K_{33}^N \end{bmatrix}\begin{bmatrix} A^{\mathrm{R}} \\ C^{\mathrm{L}} \end{bmatrix}. \tag{21}$$

Acknowledgments

The authors gratefully acknowledge the help of B. Drinkwater, P. Wilcox, and M. Caleap for valuable discussions.

References

[1] J. Gubernatis and E. Domany, "Effects of microstructure on the speed and attenuation of elastic waves in porous materials," *Wave Motion*, vol. 6, no. 6, pp. 579–589, 1984.

[2] D. Stone and B. Clarke, "Ultrasonic attenuation as a measure of void content in carbon-fibre reinforced plastics," *Non-Destruct. Test.*, vol. 8, no. 3, pp. 137–145, 1975.

[3] L. Adler, J. H. Rose, and C. Mobley, "Ultrasonic method to determine gas porosity in aluminum alloy castings: Theory and experiment," *J. Appl. Phys.*, vol. 59, no. 2, pp. 336–347, 1986.

[4] B. Ghaffari, G. Mozurkewich, L. A. Godlewski, and J. W. Zindel, "Ultrasonic characterization of shrinkage microporosity in aluminum castings," *Ultrasonics*, vol. 41, no. 9, pp. 699–707, 2004.

[5] S. Nair, D. Hsu, and J. Rose, "Porosity estimation using the frequency dependence of the ultrasonic attenuation," *J. Nondestruct. Eval.*, vol. 8, no. 1, pp. 13–26, 1989.

[6] H. Jeong and D. K. Hsu, "Quantitative estimation of material properties of porous ceramics by means of composite micromechanics and ultrasonic velocity," *NDT Int.*, vol. 29, no. 2, pp. 95–101, 1996.

[7] Q. Fan, J. Takatsubo, and S. Yamamoto, "Quantitative characterization of advanced porous ceramics based on a probabilistic theory of ultrasonic wave propagation," *J. Appl. Phys.*, vol. 86, no. 7, pp. 4023–4028, 1999.

[8] V. K. Varadan, Y. Ma, and V. V. Varadan, "A multiple scattering theory for elastic wave propagation in discrete random media," *J. Acoust. Soc. Am.*, vol. 77, no. 2, pp. 375–385, 1985.

[9] M. Caleap, B. W. Drinkwater, and P. D. Wilcox, "Modelling wave propagation through creep damaged material," *NDT Int.*, vol. 44, no. 5, pp. 456–462, 2011.

[10] V. J. Pinfield, R. E. Challis, and R. A. Smith, "A comparison of stochastic and effective medium approaches to the backscattered signal from a porous layer in a solid matrix," *J. Acoust. Soc. Am.*, vol. 130, no. 1, pp. 122–134, 2011.

[11] V. J. Pinfield and R. E. Challis, "Simulation of incoherent and coherent backscattered wave fields from cavities in a solid matrix," *J. Acoust. Soc. Am.*, vol. 132, no. 6, pp. 3760–3769, 2012.

[12] V. J. Pinfield and R. E. Challis, "Modelling the backscatter from spherical cavities in a solid matrix: Can an effective medium layer model mimic the scattering response?" *J. Phys. Conf. Ser.*, vol. 269, no. 1, art. no. 012016, 2011.

[13] I. A. Veres, D. M. Profunser, A. A. Maznev, A. G. Every, O. Matsuda, and O. B. Wright, "Point source in a phononic grating: Stop bands give rise to phonon-focusing caustics," *New J. Phys.*, vol. 14, no. 12, art. no. 123015, 2012.

[14] I. A. Veres, T. Berer, O. Matsuda, and P. Burgholzer, "Focusing and subwavelength imaging of surface acoustic waves in a solid-air phononic crystal," *J. Appl. Phys.*, vol. 112, no. 5, art. no. 053504, 2012.

[15] I. A. Veres, D. M. Profunser, O. B. Wright, O. Matsuda, and B. Culshaw, "Real-time simulations and experiments on surface acoustic wave scattering in periodic microstructures," *Chin. J. Phys.*, vol. 49, no. 1, pp. 534–541, 2011.

[16] J. Dubois, C. Aristegui, O. Poncelet, and A. L. Shuvalov, "Coherent acoustic response of a screen containing a random distribution of scatterers: Comparison between different approaches," *J. Phys. Conf. Ser.*, vol. 269, no. 1, art. no. 012004, 2004.

[17] E. H. Saenger, "Numerical methods to determine effective elastic properties," *Int. J. Eng. Sci.*, vol. 46, no. 6, pp. 598–605, 2008.

[18] M. Muller, E. Bossy, F. Meziere, and A. Derode, "2D numerical simulations of ultrasound propagation in random anisotropic media: Occurrence of two longitudinal waves in bone-like structures," in *IEEE Int. Ultrasonics Symp.*, 2011, pp. 1614–1617.

[19] L. L. Foldy, "The multiple scattering of waves. I. General theory of isotropic scattering by randomly distributed scatterers," *Phys. Rev.*, vol. 67, pp. 107–119, 1945.

[20] K. Graff, *Wave Motion in Elastic Solids*. Mineola, NY, USA: Dover, 1991.
[21] J. L. Rose, *Ultrasonic Waves in Solid Media*. Cambridge, UK: Cambridge University Press, 1999.
[22] N. G. Einspruch, E. J. Witterholt, and R. Truell, "Scattering of a plane transverse wave by a spherical obstacle in an elastic medium," *J. Appl. Phys.*, vol. 31, no. 5, pp. 806–818, 1960.
[23] W. Huang, Y. J. Wang, and S. I. Rokhlin, "Oblique scattering of an elastic wave from a multilayered cylinder in a solid. Transfer matrix approach," *J. Acoust. Soc. Am.*, vol. 99, no. 5, pp. 2742–2754, 1996.
[24] A. H. Nayfeh, "The general problem of elastic wave propagation in multilayered anisotropic media," *J. Acoust. Soc. Am.*, vol. 89, no. 4, pp. 1521–1531, 1991.
[25] L. Wang and S. I. Rokhlin, "Ultrasonic wave interaction with multidirectional composites: Modeling and experiment," *J. Acoust. Soc. Am.*, vol. 114, no. 5, pp. 2582–2595, 2003.
[26] L. Wang and S. Rokhlin, "Stable reformulation of transfer matrix method for wave propagation in layered anisotropic media," *Ultrasonics*, vol. 39, no. 6, pp. 413–424, 2001.
[27] Y. Humeida, V. Pinfield, R. Challis, P. Wilcox, and C. Li, "Simulation of ultrasonic array imaging of composite materials with defects," *IEEE Trans. Ultrason. Ferroelectr. Freq. Control*, vol. 60, no. 9, pp. 1935–1948, 2013.

Istvan A. Veres received a master's degree in civil engineering (1994–1999) from the Technical University of Budapest and a doctor of sciences (tech.) from the Institute of Mechanical Systems (IMES), Department of Mechanical Engineering, ETH Zurich. In his thesis, he investigated elastic wave propagation in wood and nondestructive testing of orthotropic materials. After a short period in the civil engineering industry, he returned to academia at the University of Strathclyde in Glasgow to work on ultrasonic wave propagation and its application in NDT. Subsequently, he has worked for RECENDT GmbH, in Linz, Austria, and at the University of Bristol. His current research interests include acoustic propagation in structured and random systems and the modeling of these phenomena both analytically and numerically. He is also involved in the development of novel optical setups for the noncontact characterization of microstructures.

Robert A. Smith is Professor of NDT and High Value Manufacturing at the University of Bristol. He studied physics at the University of Cambridge and applied acoustics at Kings College, London, with a Ph.D. degree from the University of Nottingham on the ultrasonic 3-D characterization of fiber-reinforced composites. He spent 6 years at the National Physical Laboratory and then moved to the Non-Destructive Evaluation (NDE) Group at the Royal Aerospace Establishment, Farnborough, in 1989. After several years as the Fellow in NDE at RAE, DERA, and then QinetiQ Ltd., he became a QinetiQ Senior Fellow in 2011, moving to the University of Bristol in April 2013 to commence a 5-year EPSRC Fellowship in Manufacturing entitled "NDT for High Value Manufacturing of Composites." He has authored more than 100 publications, for which he was awarded the John Grimwade Medal in 1995, 2001, 2004, 2008, and 2009, and the Roy Sharpe Prize for 1996 by the British Institute of NDT, of which he is a Fellow and President (2015–2016). He is also a Fellow of the Institute of Physics, a Chartered Physicist, and Chartered Engineer.

Valerie J. Pinfield studied natural sciences (theoretical physics) at the University of Cambridge, UK, and her Ph.D. work was carried out in the University of Leeds Food Science Department on the computational modeling of emulsion instability and ultrasonic propagation in scattering systems. Having worked for a period in research and development in the confectionery industry, she returned to academia to study ultrasonic scattering models and their application in food/pharma systems and advanced materials such as aerospace composites, first at the University of Leeds and subsequently at the University of Nottingham. Currently, her research interests are in the physical processes involved in acoustic propagation through multiphase systems, and in the modeling of such processes both analytically and numerically. She is a Lecturer in the Chemical Engineering Department at Loughborough University, UK, and is a Chartered Physicist.